Journal of the European Ceramic Society 22 (2002) 979–985

www.elsevier.com/locate/jeurceramsoc

Compressive deformation behavior of Al-doped β-SiC at elevated temperature

Sawao Honda[a,*,1], Takayuki Nagano[a,2], Kenji Kaneko[a,3], Hironori Kodama[b]

[a]*Ceramics Superplasticity Project, ICORP, Japan Science and Technology Corporation, 2-4-1, Mutsuno, Atsuta-ku, Nagoya 456-8587, Japan*
[b]*Production Engineering Research Laboratory, Hitachi Ltd., 292, Yoshida-cho, Totsuka-ku, Yokohama 244, Japan*

Received 23 April 2001; accepted 10 July 2001

Abstract

Compression tests were performed on Al-doped β-SiC fabricated by hot-pressing using pyrolyzed polycarbosilane at 2123–2223 K in He. An amorphous phase was clearly seen at the grain boundaries in as-sintered specimens. The stress exponents were from 1.1 to 1.4 in the temperature range 2123–2223 K. Strain hardening was observed under all experimental conditions. The phase transformation from β to α was not observed even after the compression tests. The amorphous phase at grain boundaries was vaporized from specimen surfaces during testing. The deformation behavior was influenced by the dynamic change of grain-boundary structure.

Keywords: Al; Creep; Grain boundary phase; Mechanical properties; SiC

1. Introduction

SiC is one of the most difficult polycrystalline materials to densify without sintering additives because of its covalent nature of Si-C bonding and its low self-diffusion coefficient. Prochazka succeeded in pressureless sintering of dense SiC with the additions of boron and carbon in 1973, with excellent strength up to 1773 K.[1] The sintering additives were added to lower grain-boundary energy and promoted the sintering process. The superior mechanical strength at elevated temperatures was achieved because the additives were incorporated into SiC grains as a solid solution.

Al has been known as an effective sintering additive since its first use by Alliegro, and SiC with the addition of Al is easily densified by hot-pressing.[2] Al increases the lattice diffusion coefficient of SiC by incorporation into SiC grains as a solid solution, which contributes to the densification in sintering. Incorporation of Al does not affect the grain growth rate proportional to the rate of grain-boundary diffusion. As a result, it is possible to obtain fine-grained SiC by Al doping.

It has been shown that Al stabilizes the 4H structure of SiC (α-SiC)[3] and there have been many reports on creep of α-SiC with the addition of Al.

Duval-Riviere and co-workers performed compressive creep tests on α-SiC which had different average grain sizes, different ratio of polytype and two Al amounts.[4] In the case of an average grain size of 1.5 μm with a grain-boundary phase, superplastic-like behavior was observed, and the grains remained equiaxed even after the compression testing. In the case of an average grain size of 3.0 μm with a grain-boundary phase, crystallographic texture from elongated grains perpendicular to the compressive axis was observed. In the case of an average grain size of 3.0 μm without a grain-boundary phase, deformation was controlled by the low mobility of grain-boundary dislocations. In other words, the critical deformation mechanism depends on the structure of the grain-boundaries in the case of average grain size between 1 and 3 μm.

Kodama and Miyoshi fabricated fine-grained β-SiC by pyrolysis of polycarbosilane (PCS).[5] The pyrolysis of PCS is usually applied to produce fine crystallites of β-SiC from its initial amorphous state. Therefore, it is possible to obtain finer-grained material in comparison with the material fabricated from commercially available powder. Even though Al was used as a sintering

* Corresponding author.
E-mail address: honda@mse.nitech.ac.jp (S. Honda).

[1] Present address: Nagoya Institute of Technology, Gokiso-cho, Showa-ku, Nagoya 466-8555, Japan.

[2] Present address: Japan Fine Ceramics Center, Mutsuno, Atsuta-ku, Nagoya 456-8587, Japan.

[3] Present address: Kyusyu University, Hakozaki, Higashi-ku, Fukuoka 812-8581, Japan.

0955-2219/02/$ - see front matter
PII: S0955-2219(01)00406-X

additive, β-SiC was formed by this fabrication process. Even though there are large numbers of reports on the creep of α-SiC with the addition of Al (grain size > 1.0 μm), there has not been any report on creep of β-SiC with the addition of Al. In the view of plastic deformation, it is assumed that β-SiC with slip plane of {111} and $<1\bar{1}0>$ is easy to deform in comparison with α-SiC with slip plane of (0001) and $<11\bar{2}0>$.

Therefore, we performed compression tests at elevated temperatures to investigate the deformation behavior of submicron-sized β-SiC with the addition of Al.

2. Experimental procedure

2.1. Specimen preparation

PCS was used as the starting material for SiC.[5] It was ground to obtain fine powders. Before pyrolyzing this powder, it was heated at 463 K for 0.5 h in the air to promote cross-linking of the polymer structure.

Pyrolyzation of the oxidized PCS was performed at 1573 K for 1 h under vacuum, and the pyrolyzed powder was mixed with 2 mol% Al powder. The mixed powders were then hot-pressed at 2173 K under vacuum with a stress of 50 MPa for 1.5 h. The relative bulk density of the as-sintered body was 99% of the theoretical density. The as-sintered body was cut by a diamond saw, and ground by diamond wheels. The size of compressive specimen was 2×2×3 mm. The specimen surfaces were finally mirror-polished with diamond paste of 1 μm.

2.2. Compression testing

Compression tests at a constant crosshead speed were conducted using an electrically controlled hydraulic machine (EHF-EG 10KN-10L, Shimazu Corp., Tokyo, Japan) at an initial strain rate from 5×10^{-4} to 1×10^{-5} s^{-1} at temperatures ranging from 2123 to 2223 K in He. The deformation of the specimen was measured from the displacement of the crosshead. The compressive direction was perpendicular to the hot-pressing direction.

True strain (ε_t) is defined as

$$\varepsilon_t = \ln(l/l_0) \quad (1)$$

where l and l_0 are the elongated and the original gage length, respectively. By assuming that there is no local necking, true stress (σ_t) can be expressed as the following relation:

$$\sigma_t = P/A_0 \exp(\varepsilon_t) \quad (2)$$

where P is the applied load and A_0 is the cross-section of the original specimen.

The strain rate ($\dot{\varepsilon}$) at elevated temperature can be expressed as[6]

$$\dot{\varepsilon} = A(\sigma^n/d^p)\exp(-Q/RT) \quad (3)$$

2.3. Microstructural change

The as-sintered material and the deformed specimens in He with surface plasma etched with CF_4+O_2 (8%) gas were observed using scanning electron microscopy (SEM: S-800, Hitachi, Tokyo, Japan). The average grain size was measured using the linear intercept length as follows:

$$d_{av} = 1.776L \quad (4)$$

where d_{av} is the average grain size and L is the linear intercept length.

X-ray analysis was also carried out to evaluate the phase transformation and the crystallization of grain-boundary phases. Also an impurity analysis was performed by inductively coupled argon plasma emission spectrophotometer and oxygen–nitrogen analyzer as shown in Table 1.

The deformed specimens were also cut perpendicular to the compressive axis, then prepared by polishing and argon-ion-beam thinning method for transmission electron microscopy (TEM) observation. High-resolution transmission electron microscopy (HRTEM) observation was performed by 200 kV TEM (EM002B, Topcon, Tokyo, Japan) with a point-to-point resolution of 0.18 nm. The grain-boundary composition was analyzed by both electron energy-loss spectroscopy (EELS) and energy dispersive X-ray spectroscopy (EDX). They were carried out on a TEM (EM002B, Topcon, Tokyo, Japan).

Electron probe micro analysis (EPMA: JXA-8600, JEOL, Tokyo, Japan) for mirror-polished cross-section of compressed specimen after cutting parallel to compressive axis was performed to evaluate the concentration distribution of grain-boundary phase.

3. Results

3.1. Mechanical behavior

The true stress–true strain curves at 2223 K for various initial strain rates are shown in Fig. 1. Flow stress increased with increasing temperature. Strain hardening was observed under all experimental conditions.

Table 1
Chemical analysis of as-sintered material

Element	wt.%
B	<0.001
Fe	0.031
Al	1.67
N	0.095
O	2.36

The true stress–true strain curves at the initial strain rate of 1×10^{-4} s^{-1} are shown in Fig. 2. Flow stress decreased with increasing temperature. Strain hardening was observed under all experimental conditions. Strain softening was observed around the true strain of −0.2 at 2123 K.

The relationship between flow stress and strain rate is shown in Fig. 3. Stress exponents were calculated from the slope of the lines. The stress exponents were from 1.1 to 1.4 in the temperature range from 2123 to 2223 K in He.

The temperature dependence of strain rate is shown in Fig. 4. The apparent activation energy was 760 kJ/mol.

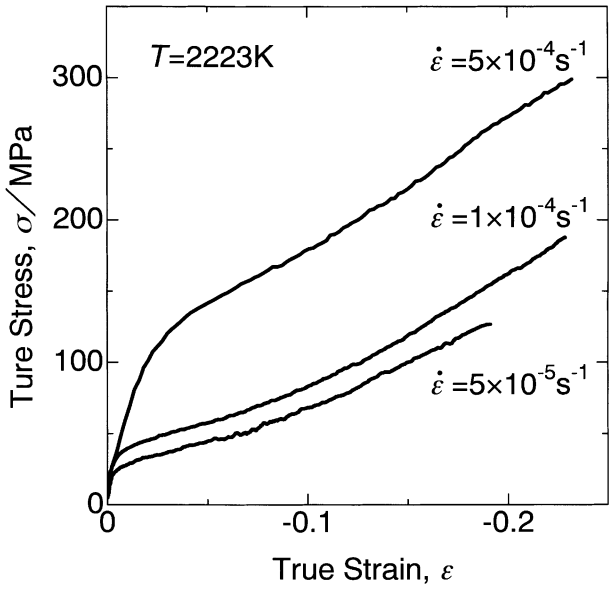

Fig. 1. True stress–true strain curves at 2223 K for various initial strain rates.

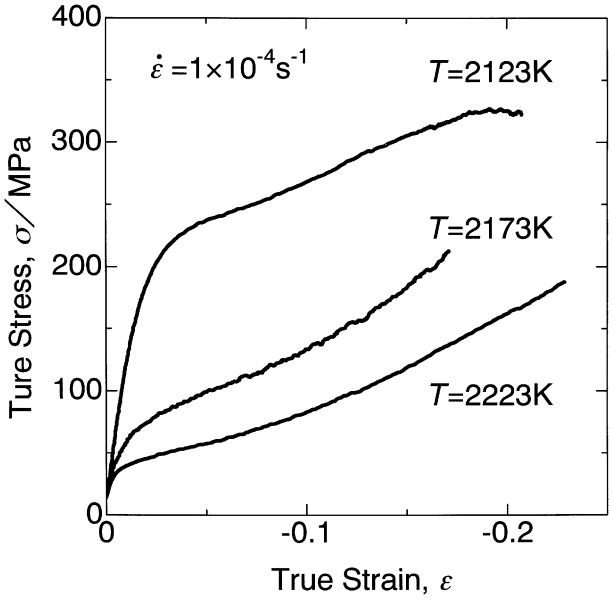

Fig. 2. True stress–true strain curves at 1E-4 s^{-1}.

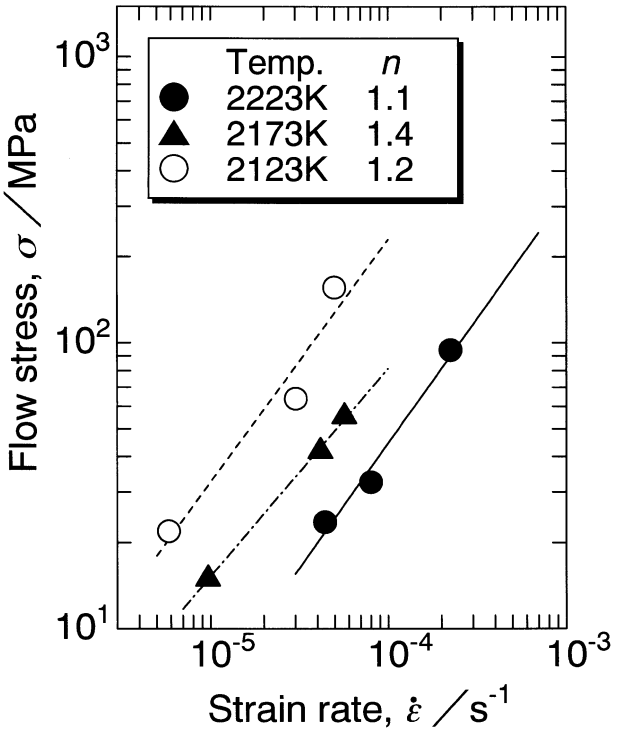

Fig. 3. Relationship between flow stress and strain rate.

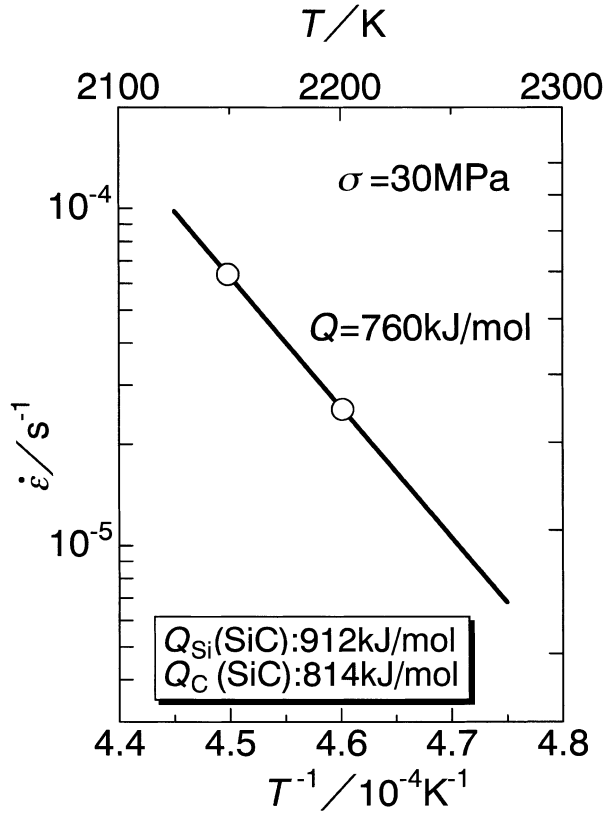

Fig. 4. Temperature dependence of strain rate.

This value is lower than that of lattice diffusion for silicon and carbon (912±5 and 814±14 kJ/mol, respectively) and higher than that of grain-boundary diffusion of carbon (569±9 kJ/mol) in high purity CVD-fabricated β-SiC.[7,8]

3.2. Microstructural change

The microstructural changes before and after compression tests are shown in Fig. 5. As-sintered body was composed of equiaxed fine grains as shown in Fig. 5(a). The amorphous phase was clearly seen at the grain boundaries. In the case of the deformed specimens, grain growth without anisotropy was observed as shown in Fig. 5(b). The grain-boundary phase seemed to be vaporized during testing. In annealed specimen corresponded to testing time, grain growth and the vaporization of grain-boundary phase were observed. The grain size after compressive deformation was almost same with that annealed specimen and strain enhanced grain growth was not observed.

High-resolution images of a grain boundary before and after the compression test are shown in Fig. 6. An

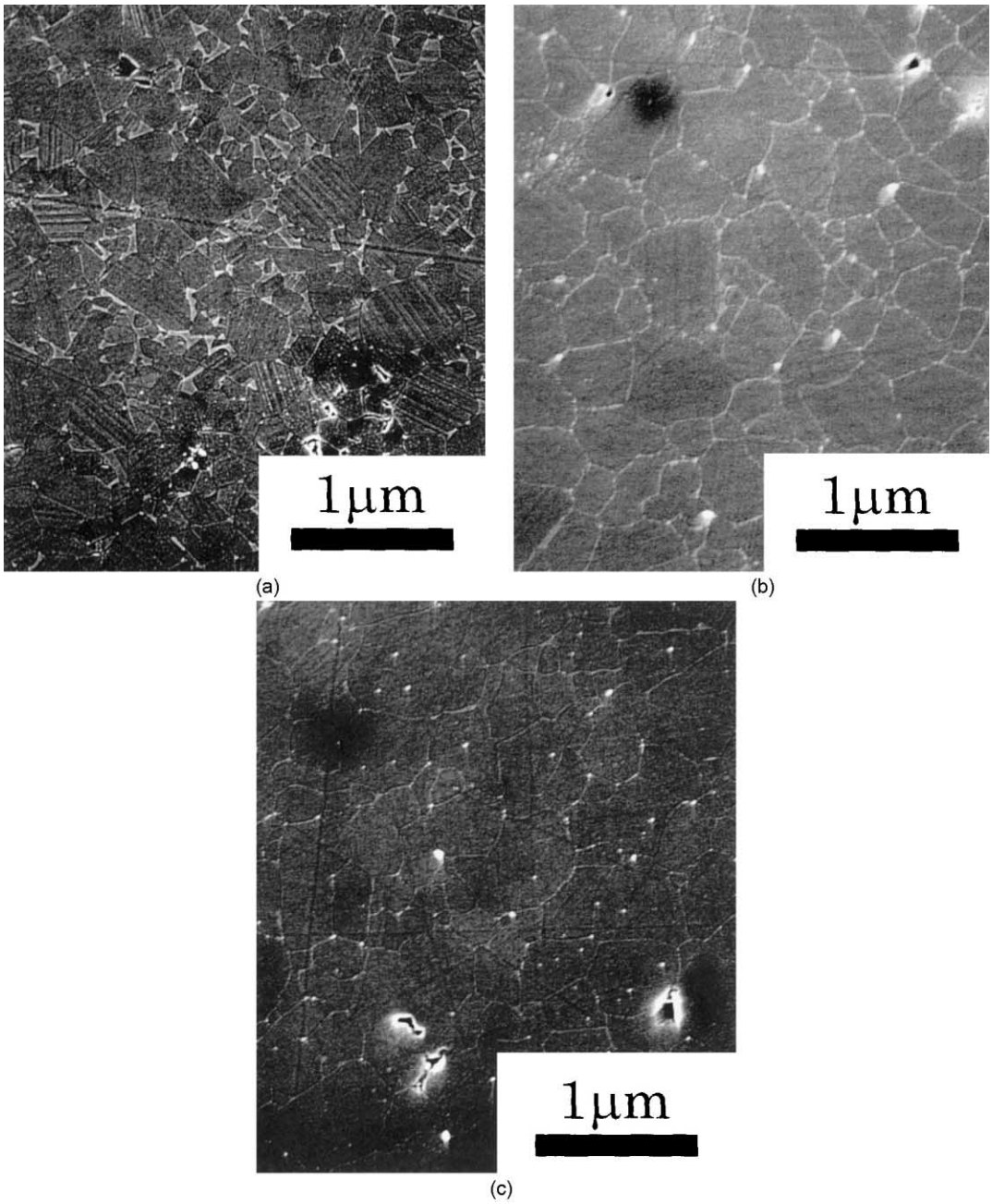

Fig. 5. SEM photographs of (a) as-sintered SiC, (b) after 20% compressive deformation at 1E-4 s^{-1} at 2223 K (compression axis is vertical) and (c) annealed specimen corresponded to testing time (20% strain, 1E-4 s^{-1}) at 2223 K.

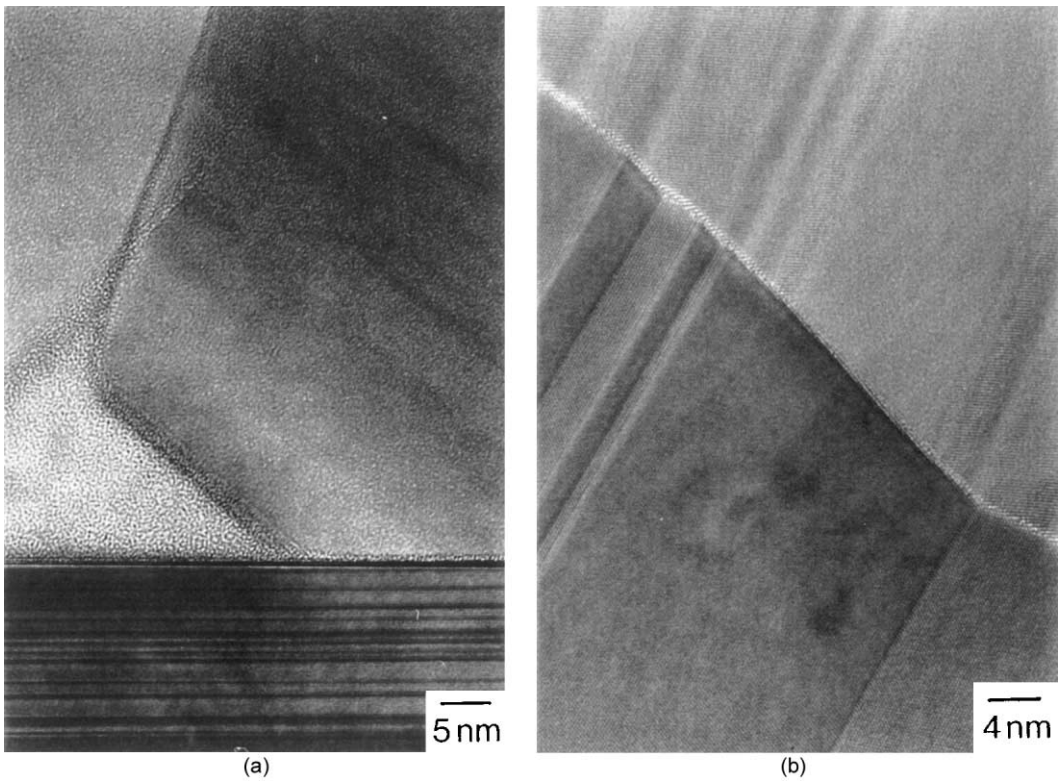

Fig. 6. High-resolution image of grain boundary in (a) as-sintered SiC, (b) after 10% compressive deformation at 5E-5 s^{-1} and 2173 K.

amorphous layer of about 0.8 nm thickness was observed in the as-sintered material. This amorphous phase was kept at the center of specimen even after compression test.

The analytical investigations of the grain and grain boundary are shown in Figs. 7 and 8. These results clearly show the segregation of Al and O at the grain boundaries, and the amorphous layer likely consisted of Si, Al, and O. Although signals from Si and C probably originated from the bulk grain, silicon carbide, an Al_2O_3–SiO_2 glass is expected at the grain boundaries judging from the energy-loss near-edge structure (ELNES) results.

The line profile, by EPMA, of the compressed specimen is shown in Fig. 9. The aluminum and oxygen concentrations were highest at the center of the specimen. The aluminum and oxygen concentrations were lower at the edges of the specimen surfaces. This result shows that the vaporization of the amorphous phase occurred from the specimen surfaces during compressive deformation.

The results of X-ray analysis before and after testing are shown in Fig. 10. In as-sintered specimen, a main phase was 3C-SiC and 2H-SiC phase was slightly observed in as-sintered specimen. In compressed specimen, 2H-SiC phase was not observed and phase transformation from β to α was not observed.

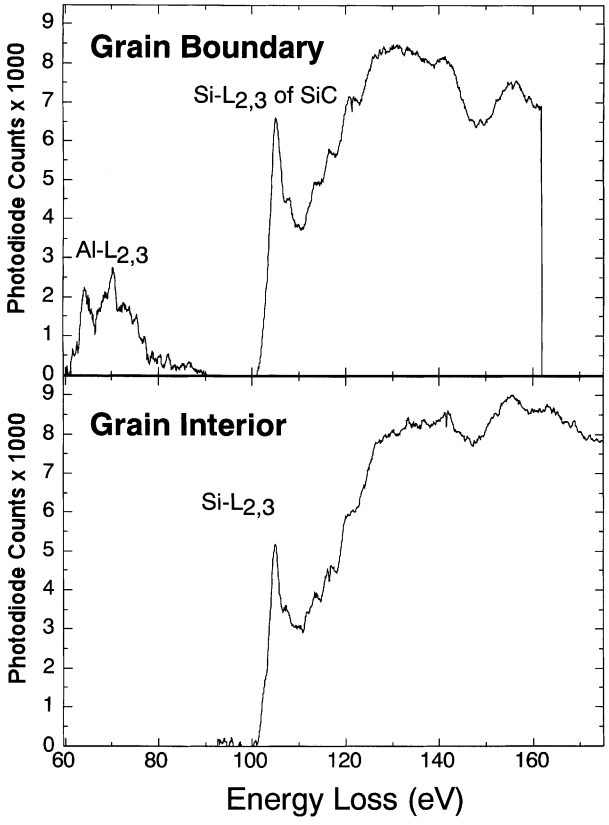

Fig. 7. ELNES results of Al–L edges and Si–L edges for as-sintered SiC at grain and grain boundary.

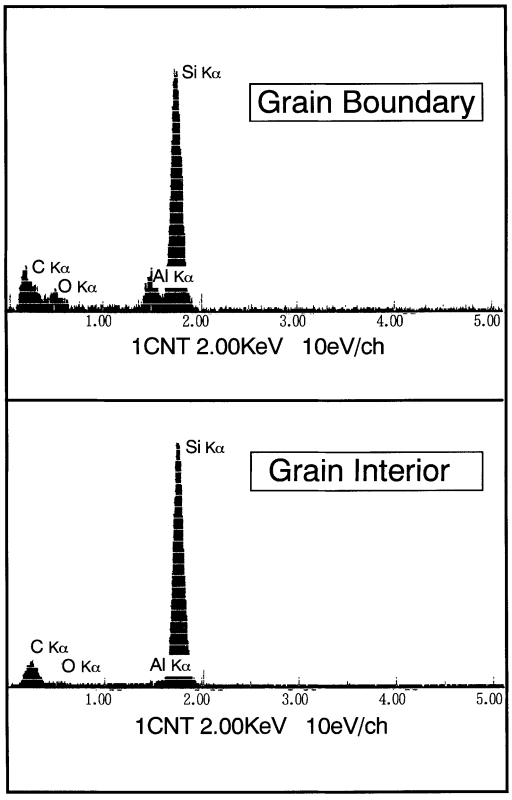

Fig. 8. EDX results for grain and grain boundary of as-sintered SiC.

4. Discussion

4.1. Effect of dynamic microstructural change on deformation behavior

Although it is known that Al exists as a solid solution in SiC grains, an amorphous phase was observed at grain boundaries. This amorphous phase was determined to be Al_2O_3–SiO_2 glass that would exist as a super-cooled liquid at temperatures higher than the glass transition temperature. Therefore, it is thought that the glass phase at the grain boundaries influences the deformation at test temperatures.

Strain hardening was thought to be caused by grain growth, vaporization of grain-boundary phase, and decomposition of SiC. The present authors reported that remarkable strain hardening by vaporization of grain boundary phase was observed in tension tests of Al-doped β-SiC.[9] The degree of vaporization of grain-boundary phase in compression test is lower than that in tension test. Therefore, remarkable strain hardening was not observed in compression tests.

In this material, the decomposition of SiC and the vaporization of additives are thought to occur at the same time at elevated temperatures as follows:[10]

$$SiC(s) + 2SiO_2(l) \rightarrow 3SiO(g) \uparrow + CO(g) \uparrow \quad (5)$$

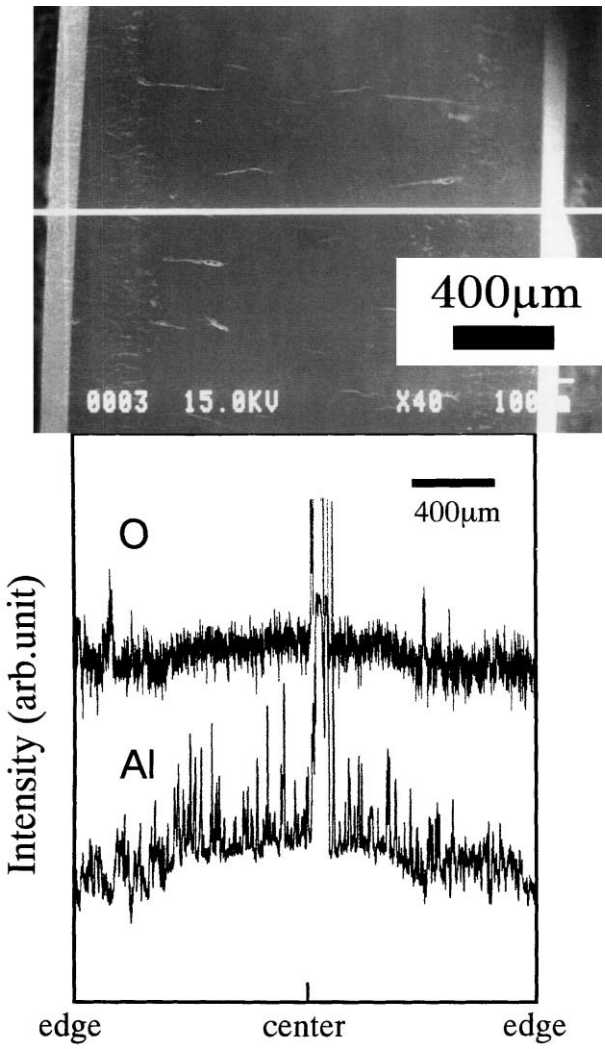

Fig. 9. Results of line analysis by EPMA for compressed specimen.

$$SiC(s) + Al_2O_3(s) \rightarrow Al_2O(g) \uparrow + SiO(g) \uparrow + CO(g) \uparrow \quad (6)$$

The present authors previously reported that these reactions occurred from specimen surfaces.[11] Therefore, the vaporization of the grain-boundary glass phase and the decomposition of SiC from specimen surfaces are thought to be the origin for the difference in morphology between specimen center and around surface in Fig. 9.

4.2. Deformation mechanisms

Grain size of the as-sintered material was 340 nm and grains retained an equiaxed shape even after compression tests in He. Moreover, neither phase transformation nor emission of dislocations were observed. It is therefore concluded that the critical deformation mechanism is grain-boundary sliding.

The possible accommodation mechanisms for the grain-boundary sliding are solution-precipitation creep,

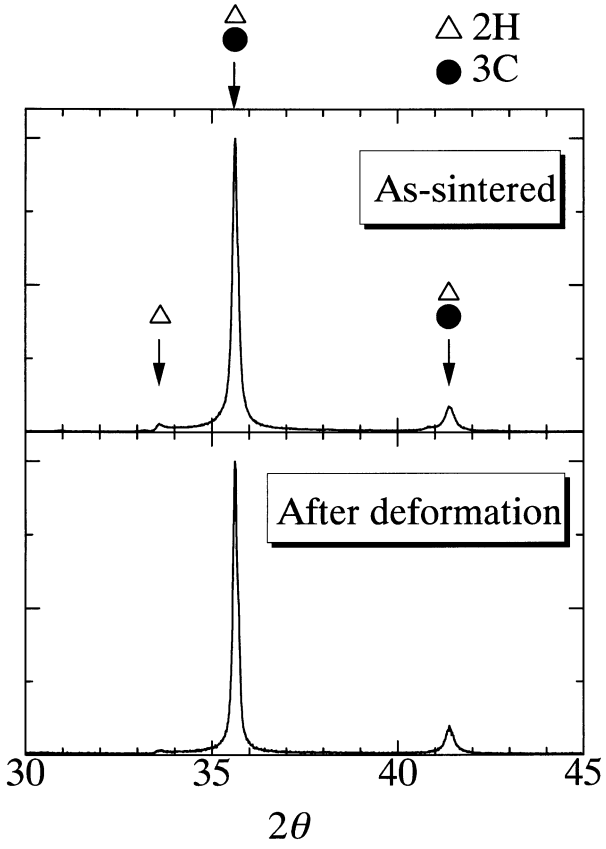

Fig. 10. Results of X-ray analysis before and after compression tests.

diffusional creep, and the re-distribution of the intergranular liquid phase. The measured value of the stress exponent ($n = 1.1$–1.4) in He was higher than the value ($n = 1$) predicted from diffusion-controlled solution–precipitation creep and diffusional creep. The higher value of the stress exponent suggests the occurrence of interface-reaction controlled processes. The inverse grain size exponent was estimated by analyzing hardening in stress-strain curves assuming that the hardening occurred due to grain growth. However, the calculated value of 4 was not consistent with the value ($P = 1$) predicted from an interface-reaction controlled process. Liquid phase must be involved with any accommodation process at the triple points. However, there is a possibility that the accommodation process at triple points changes during the compressive deformation because the grain-boundary glass phase is not stable at the deformation temperature and vaporization of the grain-boundary phase was observed at the edge of compressed specimen. Therefore, any accommodation process needs to be investigated in more detail.

5. Conclusion

Compression tests of β-SiC with the addition of 2 mol% Al at constant crosshead speed were conducted by using an electrically controlled hydraulic machine with furnace at the initial strain rates from 5×10^{-4} to 1×10^{-5} s^{-1} in a temperature range from 2123 to 2223 K in He.

1. Stress exponents were from 1.1 to 1.4 in the temperature range from 2123 to 2223 K.
2. Phase transformation and dislocation emission were not observed in deformed specimens.
3. Grains retained an equiaxed shape even after compression testing.
4. The grain-boundary phase was vaporized from specimen surfaces during tests at elevated temperatures.
5. Critical deformation mechanism was grain-boundary sliding.

References

1. Prochazka, S., The role of boron and carbon in the sintering of SiC. In *Special Ceramics 6*, ed. P. Popper. British Ceramic Research Association, Stoke-on-Trent, UK, 1975, pp. 171–181.
2. Alliegro, R. A., Coffin, L. B. and Tinklepaugh, J. R., Pressure-sintered silicon carbide. *J. Am. Ceram. Soc.*, 1956, **39**, 386–389.
3. Mitomo, M., Inomata, Y. and Kumanomido, M., The effect of doped aluminum on thermal stability of 4H- and 6H-SiC. *Yogyo-Kyokai-Shi*, 1970, **78**, 224–228.
4. Duval-Riviere, M. L., Carry, C. and Vicens, J., Microstructural study of deformation mechanisms in polycrystalline α-SiC deformed at high temperature. *Phy. Stat. Sol.*, 1996, **155**, 63–82.
5. Kodama, H. and Miyoshi, T., Study of fracture behavior of very fine-grained silicon carbide ceramics. *J. Am. Ceram. Soc.*, 1990, **73**, 3081–3086.
6. Mukherjee, A., Bird, J. E. and Dorn, J. E., Experimental correlations for high-temperature creep. *Trans. ASM*, 1969, **62**, 155–179.
7. Hon, M. H. and Davis, R. F., Self-diffusion of ^{14}C in polycrystalline β-SiC. *J. Mater. Sci.*, 1979, **14**, 2411–2421.
8. Hon, M. H., Davis, R. F. and Newberry, D. E., Self-diffusion of ^{30}Si in polycrystalline β-SiC. *J. Mater. Sci.*, 1980, **15**, 2073–2080.
9. Nagano, T., Kaneko, K. and Kodama, H., Tensile ductility of Al-doped β-silicon carbide at elevated temperature. In *Proc. of the Third Pacific Rim International Conference on Advanced Materials and Processing (PRICM3)*, ed. M. A. Imam, R. DeNale, S. Hanada, Z. Zhong and D. N. Lee. Minerals, Metals, and Materials Society (TMS), Warrendale, PA, 1998.
10. Grande, T., Sommerset, H., Hagen, E., Wiik, K. and Einarsrud, M.-A., Effect of weight loss on liquid-phase sintered silicon carbide. *J. Am. Ceram. Soc.*, 1997, **80**, 1047–1052.
11. Nagano, T., Kaneko, K., Zhan, G.-D. and Mitomo, M., Effect of atmosphere on weight-loss of sintered silicon carbide during heat treatment. *J. Am. Ceram. Soc.*, 2000, **83**, 2781–2787.